J Electroceram (2010) 25:70–76
DOI 10.1007/s10832-009-9590-y

Textured ferroelectric $SrBi_2Nb_2O_9$ phase obtained by *melt-quenching the* $SrBi_2B_2O_7$-Nb_2O_5 system and its anisotropic dielectric and pyroelectric properties

Koushik Majhi · K. B. R. Varma

Received: 17 March 2009 / Accepted: 16 September 2009 / Published online: 2 October 2009

Abstract Textured $SrBi_2Nb_2O_9$ ceramics were obtained by quenching the melts of $SrBi_2B_2O_7$-Nb_2O_5 in equimolar ratio. The as-quenched samples were crystalline comprising 40% c-oriented grains. The influence of the post heat-treatment temperature on the orientation factor (*f*) and microstructure was studied using x-ray powder diffraction (XRD) and Scanning electron microscopy (SEM). The orientation factor was found to increase with increasing post heat-treatment temperature and reached a maximum value of 65% for the samples heated at 700°C for 10 h. Relative density and the grain-size of the partially grain oriented ceramics were found to increase with an increase in the heat-treatment temperature. The effect of texturing yielded anisotropy in the dielectric and pyroelectric properties. The dielectric constant $\left(\varepsilon_r'(\perp) = 114\right)$ and the pyroelectric coefficient ($p(\perp)$= -0.07 nC cm^{-2} °C^{-1}) along the direction perpendicular to the melt pressing axis were superior to that of the direction parallel ($(\varepsilon_r'(\|) = 93)$ ($p(\|)$=-0.02 nC cm^{-2} °C^{-1})) (c-axis of the grain) to the pressing axis at room temperature.

Keywords Texture · Dielectric · Pyroelectric · Aurivillius oxides · Ferroelectric

1 Introduction

Aurivillius family of ferroelectric oxides associated with a general chemical formula $Bi_2A_{n-1}B_nO_{3n+3}$ possess an anisotropic crystal structure containing alternate $[Bi_2O_2]^{2+}$and n perovskite $[A_{n-1}B_nO_{3n+1}]^{2-}$ layers [1]. These materials have attracted much attention owing to their potential non-volatile random access memory (NVRAM) [2] and high temperature piezo-electric [3] applications. However, the volatile nature of bismuth oxide makes the growth of stoichiometric single crystals of these materials very difficult and the ceramics comprising randomly oriented crystallites show poor polar properties. Further, the two dimensional nature of the ferroelectric switching makes the poling very difficult. In general, theses problems are overcome by adding suitable additives which are often used for lowering the heat-treatment temperature and engineering the microstructures of the electroceramics [4–11]. In this study the glassy phase (B_2O_3 which evolves as a result of the reaction between $SrBi_2B_2O_7$ and Nb_2O_5) is a well known liquid former. The glassy phase in ceramics was reported to form grain-to-grain bridge via liquid phase formation during heat-treatment. This would facilitate the grain growth and help in getting the inter-grain pores eliminated [12, 13]. It was also known that the physical properties of a ceramic could be made anisotropic by tailoring the microstructure, where the grain orientation is an important aspect. In the case of textured ceramics the grains are oriented in a particular crystallographic direction and the ceramic exhibits enhanced physical properties when the measurement is carried out in the direction of the orientation of the polar axis. In randomly oriented grains, the contribution from the permanent dipoles is averaged out and the properties are isotropic. Aurivillius family of oxides which have layered structure, the dielectric polarization is higher in the a-b plane and the contribution from the c-axis or the plane perpendicular the bismuth oxide layer is less significant. Grain orientation in electroceramics was achieved through various techniques such as hot forging [14], hot pressing [15], cold pressing [16], melt-quenching [17] and templated grain growth (TGG) via tape casting [18–20]. TGG is the most widely used technique which involves orienting anisotropi-

K. Majhi · K. B. R. Varma (✉)
Materials Research Centre, Indian Institute of Science,
Bangalore 560 012, India
e-mail: kbrvarma@mrc.iisc.ernet.in

cally shaped template particles via tapecasting in a dense fine grained matrix. This method has been used to fabricate textured ceramics of several materials such as mullite [21], $Sr_{0.53}Ba_{0.47}Nb_2O_6$ [18], $Bi_4Ti_3O_{12}$ [22, 23] and $SrBi_2Nb_2O_9$ [24–26].

In the present work, we report the evolution of {00 l} textured $SrBi_2Nb_2O_9$ (SBN) ceramics from a reactive $SrBi_2B_2O_7$ (SBBO) [27, 28]-Nb_2O_5 system. Simple melt-quenching of this system has yielded partially grain oriented SBN ceramics. Indeed, the melt-quenching method was widely used to fabricate textured ceramics of many Bi based high temperature superconductors [17, 27]. SBN is an n=2 member of Aurivillius family of oxides associated with relaxor characteristics [29–31]. To the best of our knowledge, there are no details reported in the literature concerning the direct method of fabricating SBN ceramics (grain oriented) using a reactive glass matrix. The effect of post heat-treatment temperature on the degree of grain orientation and the microstructure was investigated. The dielectric and pyroelectric properties that were studied along two different directions, (parallel and perpendicular to the pressing axis) of the as-quenched/post annealed samples were found to be anisotropic.

2 Experimental

The textured SBN ceramics were fabricated by quenching the melts of $SrBi_2B_2O_7$ and Nb_2O_5 in equimolar ratio. These were prepared by a two step process. The first step was the fabrication of glasses in the composition SrO-Bi_2O_3-B_2O_3 which is expected to yield $SrBi_2B_2O_7$ crystalline phase on heat-treatment. Constituent carbonates/ oxides ($SrCO_3$, Bi_2O_3, and H_3BO_3 (Aldrich chemicals)) in stoichiometric ratio were mixed well using a pestle and mortar. The resultant mixture was packed into a platinum crucible and melted at 1100°C using a Lenton glass melting (EHF) furnace. The melt was held at this temperature for about 60 min for homogenization and then poured over a stainless steel plate and was pressed by another plate. The resultant product was a transparent glass plate of about 50 mm in dia and 2 mm to 3 mm in thickness. The glassy nature of the as-quenched plate was confirmed by differential scanning calorimetric studies. The powders were ground by using an agate mortar and a pestel. Before grinding, the mortar and the pestel have been cleaned thoroughly and dried using acetone. In the second step, well mixed powders containing equimolar ratio of reagent grade Nb_2O_5 and the above $SrBi_2B_2O_7$ glass powder were melted at 1100°C/1 h in the platinum crucible. The process of quenching the melt described above was repeated which enabled us to obtain 4 mm to 5 mm thick optically opaque plates. The phase analysis of the as-quenched plate was carried out using x-ray powder diffraction (XRD) (Philips PW1050/37 diffractometer (Cu-K_α radiation)) technique at room temperature. The as-quenched samples were heated at different temperatures ranging from 500°C to 800°C for 10 h. The phase formation and the crystallographic texture of the heat-treated samples were examined by XRD. The degree of orientation ({00 l} in the present case) was calculated using Lotgering's method, in which the orientation factor (f) was obtained using the formula,

$$f = \frac{(p - p_0)}{(1 - p_0)}$$

where $p = \Sigma I_{(00l)} / \Sigma I_{(hkl)}$ for the textured sample and $p_o = \Sigma I_{(00l)} / \Sigma I_{(hkl)}$ for the randomly oriented SBN powder prepared via the conventional solid state reaction route. ΣI_{00l} is the sum of x-ray intensities, reflected from the {00 l} family of planes and ΣI_{hkl} is the sum of the reflected x-ray intensities from all the planes. The scanning electron microscope (SEM) (FEI Quanta 200 FEG) was employed for carrying out the microstructural analysis of the as-quenched as well as heat-treated samples. The densities of the samples were determined by Archimedes's method with Xylene (density, ρ=0.87 g/cm^3) as the liquid media. For electrical characterization, the samples (as-quenched and the heat-treated) were cut and ground into two types of discs; one with the direction of measurement parallel (SBN$\parallel$) and the other, perpendicular (SBN$^{\perp}$) to the pressing axis of the as-quenched virgin plate. For electroding, the polished surfaces were sputtered with gold and silver leads were bonded using silver epoxy. Capacitance measurements were carried out using a HP 4194A impedance–gain phase analyzer as a function of frequency (100 Hz to 1 MHz) and temperature (room temperature to 400°C). The direct method (Byer and Roundy) was employed for making pyroelectric current measurements. For this, the samples were connected to a Keithley 485 auto ranging picoammeter and the pyroelectric current was monitored as a function of temperature (room temperature to 400°C) at a heating rate of 3 C/min. The pyroelectric coefficient 'p' was evaluated using the relation,

$$p = \frac{I}{A\left(\frac{dT}{dt}\right)}$$

where I is the pyroelectric current, A is the electroded area of the sample and dT/dt is the heating rate.

3 Results and discussion

3.1 XRD and texture analysis

The XRD patterns recorded for the as-quenched and heat-treated flat plates are depicted in Fig. 1(b–e). The XRD

pattern of the SBN ceramic powder synthesized via the conventional solid state reaction route is also illustrated in Fig. 1(a) for comparison. The XRD pattern obtained for the as-quenched sample [Fig. 1(b)] clearly reveals the presence of intense Bragg peaks corresponding to that of the SBN layered perovskite. The reaction scheme that is proposed based on this result is as follows

$$SrBi_2B_2O_7(glass) + Nb_2O_5 \xrightarrow{\text{melt quench}} SrBi_2Nb_2O_9(crystalline) + B_2O_3.$$

The broadness that is associated with these peaks indicate the fine grained nature of the as-quenched ceramics. Another interesting aspect of this pattern is that the x-ray peaks corresponding to {00 l} reflections are more prominent unlike in the case of ceramic powder prepared via the conventional solid-state reaction route. Since there are no Bragg peaks corresponding to crystalline B_2O_3, (B_2O_3 formation is expected as a result of the chemical reaction between SBBO and Nb_2O_5) we believe that this may be in amorphous phase, probably segregated at the grain boundaries. Since all the XRD peaks corresponding to the known SBN phase, the incorporation of B_2O_3 in the lattice is ruled out. The Lotgering's factor ({00 l} reflections) for the as-quenched sample was calculated to be around 0.4 implying that 40% of the grains in the matrix are c-oriented. The XRD patterns for the samples heat-treated at 500°C, 700°C and 800°C for 10 h are shown in Fig. 1(c–e). In these patterns, the intensities

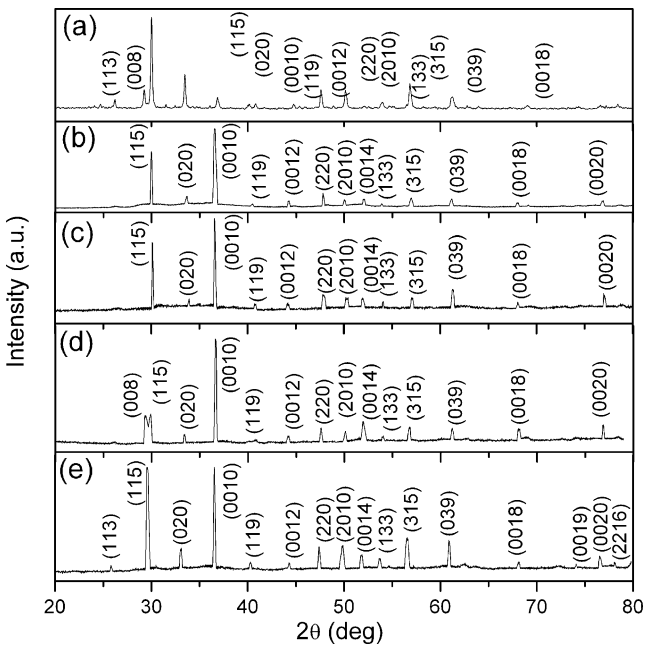

Fig. 1 XRD patterns (**a**) SBN powder prepared by solid state reaction route, (**b**) as-quenched plate (**c**–**e**) quenched plates heat-treated at 500°C, 700°C, and 800°C for 10 h respectively

corresponding to the {00 l} planes of SBN dominate. The degree of {00 l} texture increases with increase in heat-treatment temperature. Figure 2 shows the variation of Lotgering's factor (f) as a function of sintering temperature. The value of f increases from 0.52 to 0.65 when the heat-treatment temperature was raised from 500°C/10 h to 700°C/10 h. This suggests that, during the process of heat-treatment, the grain growth occurs in a preferential direction whose major faces are parallel to the plane of the ceramic plate and perpendicular to the pressing axis. However, for the samples heat-treated at 800°C/10 h, the ***f*** value decreases suggesting that the threshold temperature for accomplishing maximum ***f*** value is 800°C. Interestingly even at this stage of heat-treatment, no x-ray peaks pertaining to the crystalline B_2O_3 phase (which is expected as a result of the chemical reaction between $SrBi_2B_2O_7$ and Nb_2O_5) are noticeable in the XRD patterns. The samples sintered at 700°C/10 h which showed higher ***f*** value were selected for subsequent physical property measurements. The mechanism responsible for this kind of texturing is not very evident as there is no significant temperature gradient that is provided across the sample during the process of heat-treatment. Normally texturing in ceramics is achieved with the aid of externally added template particles. In the present case, 65% orientation in the grains is accomplished in the absence of such starting particles. Therefore, one possible explanation is that the plate shaped crystallites would have readily formed parallel to the surfaces of the two metal plates (act as heat sinks) as the melt is squeezed between them. Also, there is a possibility for the incidence of two dimensional crystallization along the metal plate–melt interface during the process of pressing. These oriented crystallites of significant volume fraction would possibly act as template particles and facilitate the growth of oriented crystallites. The texture development in the ceramics with preexisting template particles is a well established process. In the process of sintering, the coarsening of template particles occurs in which the matrix grains which are misaligned with the template particles form high energy boundaries and are easily consumed by the templates. The grains oriented parallel to the templates form low-energy grain boundaries with the templates and are not consumed by the template particles. In effect the volume fraction of the {00 l} oriented grains increases at the expense of the disoriented grains. In the present studies, the percentage of grain orientation achieved for the SBN ceramics is less than that of the textured ceramics of other Aurivillius oxides fabricated via templated grain growth [24–26]. We believe that {00 l} oriented grains that form while quenching serve as templates through out the sample. Indeed, the texture of the ceramics was not confined to the surface as it was confirmed to exist at different depths from the surface by XRD studies. However, the ***f*** is found to decrease (slightly) as a function of the depth of the sample.

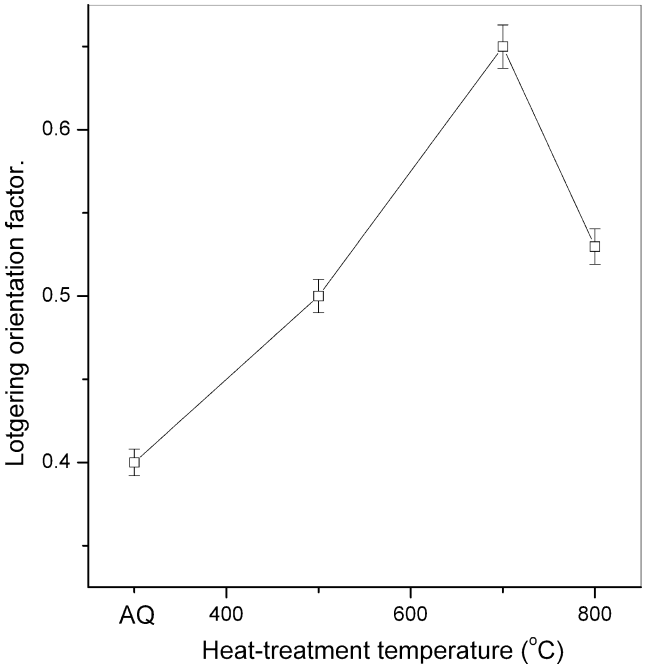

Fig. 2 Variation of Lotgering's factor (*f*) as a function of heat-treatment temperature, where AQ denotes as-quenched sample

3.2 Microsctrctural studies

Figure 3(a–c) shows the scanning electron micrographs recorded for the surfaces parallel (SBN‖) to the plane of the plate for the as-quenched and samples heat-treated at 700°C for 10 h. The microstructure corresponding to the as-quenched sample (Fig. 3 (a)) shows the presence of relatively slim grains associated with some amount of orientation. However, it is evident from Fig. 3(b) that most grains are aligned such way that their large faces are parallel to the a-b planes. They are preferentially aligned along the plane perpendicular to the pressing direction and parallel to the surface of the as-quenched plate. Figure 3(c) depicts the cross-sectional view (⊥ to the quenching direction) of the sample heat-treated at 700°C for 10 h. The micrograph corresponding to the cross-section (normal to the pressing direction) of the sample heat-treated at 700°C/10 h depicted in Fig. 3(c) clearly demonstrates the randomness in the arrangement of the platy grains. The grains are characterized by a uniform thickness of about 1 μm to 2 μm and with an average length of about 40–50 μm which is higher than the average grain size that is normally observed in the case of pure SBN ceramics obtained by solid-state reaction route. These results are consistent with those obtained by XRD analyses. The abnormal grain growth is attributed to the presence of glassy B_2O_3 (which acts as a flux). Figure 4 shows the variation of relative density as a function of sintering temperature. The as-quenched sample (AQ) showed a poor relative density of about 77%. Due to this, the as-quenched samples were mechanically not strong. However, the post heat-treated samples showed improved density and increases with increase in heat-treatment temperature. The relative density of the sample heat-treated at 500°C was about 88% and reached a maximum value of about 95% for the sample heat-treated at 700°C. The increase in the relative density of the ceramics is ascribed to the elimination of intergranular porosity with the increase in heat-treatment temperature. Interestingly, the observed relative density is comparable to that of the SBN ceramics sintered using the powders prepared via solid-state reaction route where densities of only about 92–93% could be achieved. But nevertheless, the relative density is found to decrease with increase in the heat-treatment temperature beyond 700°C which is attributed to the exaggerated grain growth accompanied by entrapped intragranular pores. Higher temperatures of heat-treatment resulted in a rapid grain growth at a rate much faster than the rate of entrapped porosity leading lower density. Also the loss of B_2O_3 at elevated temperature is not completely ruled out. Whereas at lower temperatures this could act as a flux and assist in enhancing the materials transport as the B_2O_3 wets the grains of the matrix materials. In such a case, transient glassy phase (B_2O_3) formed at lower

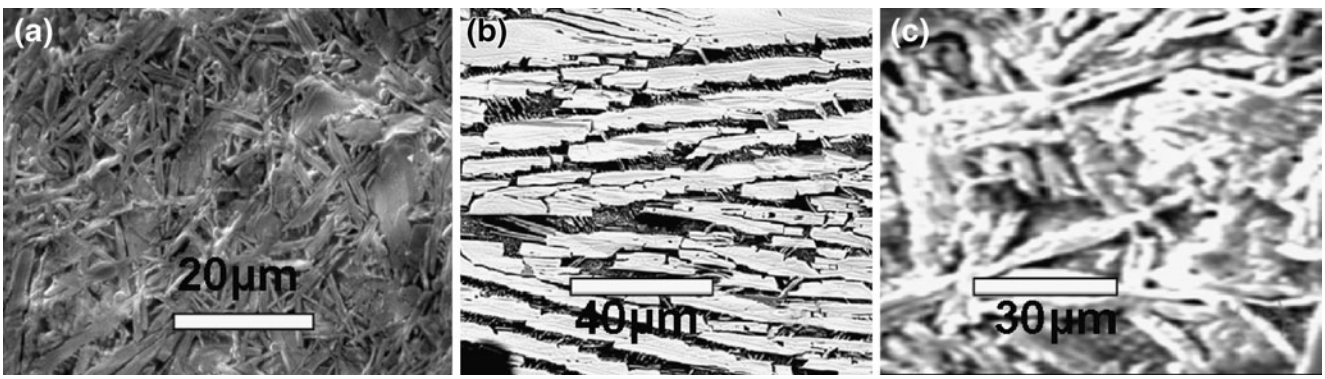

Fig. 3 Scanning electron micrographs of the (**a**) as-quenched sample (**b**) Surfaces of the sample heat-treated at 700°C, for 10 h respectively and (**c**) cross-sectional view of the sample heat-treated at 700°C/10 h

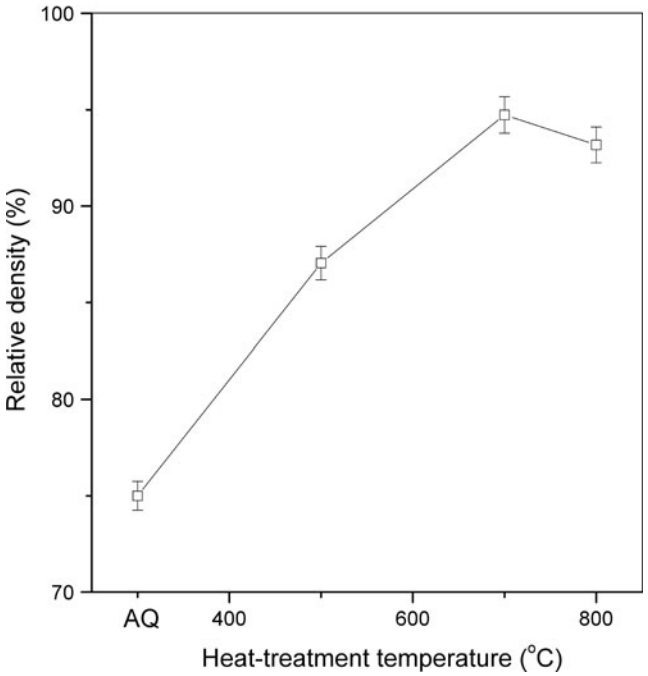

Fig. 4 Variation of relative density of SBN plates as a function of heat-treatment temperature, where AQ denotes the as-quenched sample

temperatures would facilitate the densification via pore elimination process.

3.3 Dielectric anisotropy

Figure 5(a, b) shows the temperature dependence of the dielectric constant (ε_r') and dielectric loss (D) measured at 1 MHz for the textured SBN∥ and SBN$^{\perp}$ samples heat-treated at 700°C for 10 h. Both the SBN∥ and SBN$^{\perp}$ samples exhibit the characteristic diffuse phase transition which is akin to that of the SBN ceramic fabricated via the conventional route. Interestingly, a significant anisotropy in the dielectric constant was observed throughout the temperature range covered in the present studies. The dielectric constant of the sample SBN$^{\perp}$ $(\varepsilon_r' = 114)$ is higher than the one obtained for the sample SBN∥ $(\varepsilon_r' = 93)$ at room temperature. The dielectric anisotropy in the dielectric constant is maximum around the temperature of the dielectric constant maximum (T_m). The observed loss which is depicted in Fig. 5(b) has almost the same value for both the orientations at temperatures lower than 400°C. The loss for SBN∥ increases more rapidly than that of the SBN$^{\perp}$ at high temperatures (>450°C). In SBN, the polar axis lies in the a-b plane. Therefore, the higher ε_r' encountered in the case of SBN$^{\perp}$ is justified. Nearly more than half the grains are oriented with their polar axes lying parallel to the applied field direction in the samples that were cut perpendicular to the pressing axis. The observed higher values of loss (D) especially, at high temperatures in the case of SBN∥ samples, may be attributed to higher electrical conductivity associated with the c-axes of the grains.

The effect of crystallographic texture on the diffuseness of the phase transition has been studied by estimating the degree of diffuseness (γ) using the following empirical relation [32],

$$\frac{1}{\varepsilon_r'} = \frac{1}{\varepsilon_m'} + (C)^{-1}(T - T_m)^{\gamma}$$

Where ε_m' is the maximum value of the dielectric constant at the transition temperature (T_m), C is the Curie-like constant and γ signifies the diffuseness of the transition. The limiting values 1 and 2 for γ respectively reduce the expression to the Curie–Weiss law valid for a normal and the quadratic dependence valid for the ideal relaxor ferroelectric. The slope of the log $\left(1/\varepsilon_r' - 1/\varepsilon_m'\right)$ and log $(T-T_m)$ plot gives the value for γ. Figure 6 shows the typical plots obtained for both the SBN∥ and SBN$^{\perp}$ samples. The value of the degree of diffuseness for SBN$^{\perp}$ sample is 1.4 while it is 0.86 for the SBN∥ sample. The decrease in the value of γ from 1.4 to 0.86 implies that there is decrease in the diffuseness of the transition. It is tentatively concluded based on this result that the texturing renders ordering of the dipoles in the present samples.

3.4 Anisotropy in pyroelectric coefficient

The effect of texturing on the polar nature of the ceramics could be directly visualized via the pyroelectric property

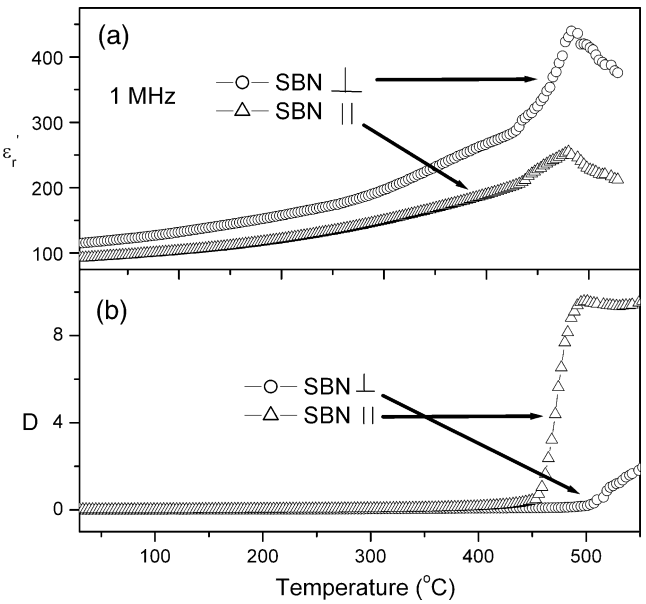

Fig. 5 Variation of (**a**) dielectric constant (ε_r') and (**b**) dielectric loss (D) as a function of temperature at 1 MHz for two different orientations

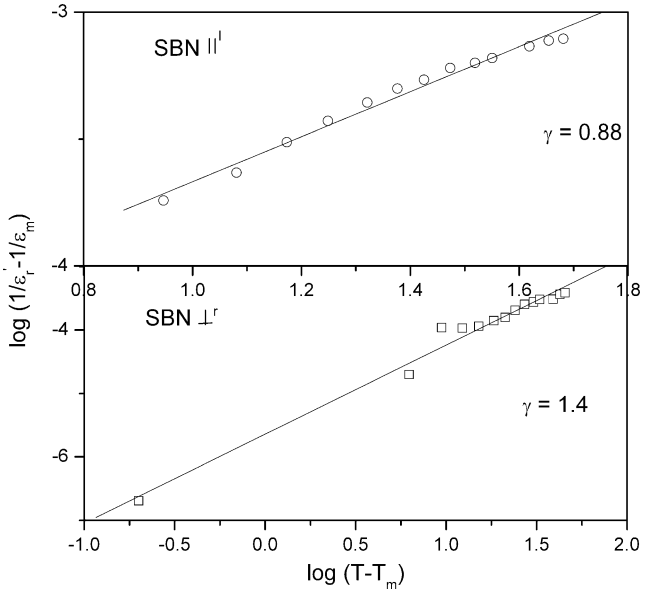

Fig. 6 Variation of log $\left(1/\varepsilon_r' - 1/\varepsilon_m'\right)$ with log $(T-T_m)$ for two different orientations

measurements. Figure 7 shows the variation of pyroelectric coefficient (p) as a function of temperature for both the SBN∥and SBN⊥ samples. Pyroelectric coefficient increases with increase in temperature for both the samples and exhibit anomalies around 470°C, which is consistent with the relaxor to paraelectric transition temperature (T_m) of the SBN ceramics [30]. The room temperature value of the SBN⊥ pyroelectric coefficient (−0.07 nC cm^{-2} °C^{-1}) was found to be higher than that of SBN∥ sample (−0.02 nC cm^{-2} °C^{-1}). The observed anisotropy is well pronounced in the vicinity of relaxor to paraelectric transition where the values of the pyroelectric coefficients for SBN∥ and SBN⊥samples are −0.34 nC cm^{-2} °C^{-1} and −1.39 nC cm^{-2} °C^{-1} respectively. The pyroelectric coefficients are negetive in the entire range of the temperatures under study for both the ceramics. In general, the pyroelectric coefficient measured consists of two components. The primary effect arising due to the change in spontaneous polarization (P_s) which is large and negative as it decreases with increasing temperature. The secondary effect has piezoelectric origin. It is also known that in ferroelectric ceramics and single crystals, both the primary and total pyroelectric effects are large and negative. The relatively large and negative value of the pyroelectric coefficient implies that the contribution from the secondary pyroelectric effect is insignificant. In many ferroelectric oxides, the secondary effects dominates which lead to the positive values of pyroelectric coefficients. For instance, the textured $Sr_xBa_{1-x}Nb_2O_6$ ceramics were found to show high positive values of pyroelectric coefficients [33, 34]. Apart from these effects, the presence of space charges and surface charges may significantly contribute to the bulk polarization of the ceramics especially, when there is a finite electrical conductivity associated with them. In the case of relaxor ferroelectrics with finite electrical conductivity, the pyroelectric current has a complex character and was found to exhibit a broad anomaly in the temperature region of relaxor to paraelectric transition [35]. The pyroelectric behavior and the anomaly observed for the textured SBN in the present study could be attributed only to the primary pyroelectric effect. The anisotropy in the pyroelectric effect that is encountered in partially grain oriented SBN ceramics obtained by melt-quenching the $SrBi_2B_2O_7$-Nb_2O_5 system is interesting from both the academic as well as technological applications point of view. Indeed this phenomena is consistent with that of the dielectric anisotropy that is observed in the present studies.

4 Conclusions

Significant anisotropies in both the dielectric constant and the pyroelectric coefficients were encountered in the SBN ceramics fabricated by melt-quenching $SrBi_2B_2O_7$-Nb_2O_5 system followed by appropriate heat-treatment. The anisotropy especially in the pyroelectric coefficient is appreciably high in the vicinity of the phase transition temperature. The dielectric and pyroelectric properties were found to be superior in the direction perpendicular to the quenching direction. These are attributed to the presence of partial

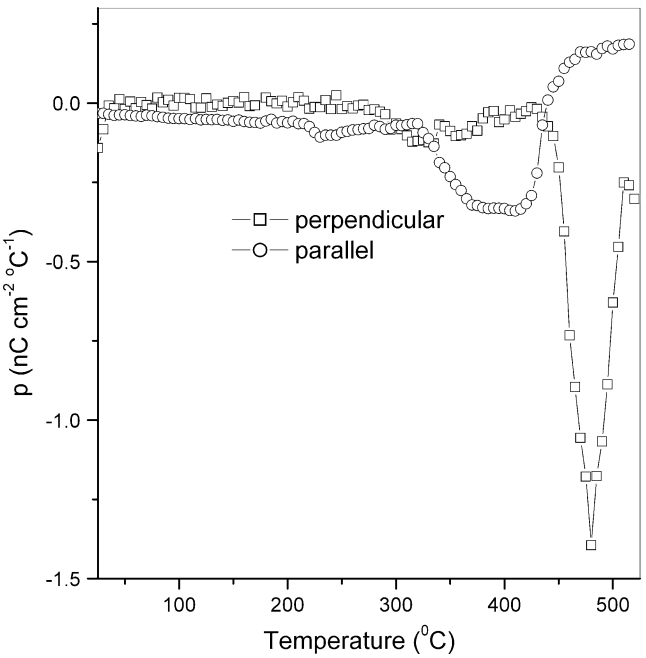

Fig. 7 Variation of pyroelectric co-efficient (p) as a function of temperature for two different orientations

grain orientation which enhances the contribution from the polar a–b plane.

References

1. R.E. Newnham, R.W. Wolfe, J.F. Dorrian, Mater. Res. Bull. **6**, 1029 (1971)
2. W.L. Warren, B.A. Tuttle, D. Dimos, Appl. Phys. Lett. **67**, 1426 (1995)
3. D. Damjanovic, Curr. Opin. Solid State Mater. Sci. **3**, 469 (1998)
4. S.-F. Wang, T.C.K. Yang, Y.-R. Wang, Y. Kuromitsu, Ceram. Int. **27**, 157 (2001)
5. S.K. Sarkar, M.L. Sharma, Mater. Res. Bull. **24**, 773 (1989)
6. T. Takada, S.F. Wang, S. Yoshikawa, S.-J. Jang, R.E. Newnham, J. Am. Ceram. Soc. **77**, 2485 (1994)
7. S.-W. Kim, H.-P. Jeon, S.-K. Lee, D.-K. Choi, Mater. Chem. Phys. **94**, 185 (2005)
8. J.-M. Yoon, J.-A. Lee, J.-H. Lee, J.-J. Kim, S.-H. Cho, J. Eur. Ceram. Soc. **26**, 2129 (2006)
9. J.-A. Lee, J.-H. Lee, J.-J. Kim, J. Eur. Ceram. Soc. **26**, 2135 (2006)
10. K.P. Surendran, P. Mohanan, M.T. Sebastian, J. Solid State Chem. **177**, 4031 (2004)
11. P.V. Bijumon, M.T. Sebastian, Mater. Sci. Eng. B **123**, 31 (2005)
12. Kingery, J. Appl. Phys. **30**, 301 (1959) doi: 10.1063/1.1735155
13. W.D. Kingery, M.D. Narasimhan, J. Appl. Phys. **30**, 307 (1959)
14. M. Venet, A. Vendramini, I.A. Santos, J.A. Eiras, D. Garcia, Mater. Sci. Eng. B **117**, 254 (2005)
15. J. Rodel, A.M. Glaeser, J. Am. Ceram. Soc. **73**, 3292 (1990)
16. K. Shantha, K.B.R. Varma, Mater. Res. Bull. **32**, 1581 (1997)
17. S.J. Peng, M.D. Lan, P. Klavins, J.Z. Liu, R.N. Shelton, Physica C **212**, 301 (1993)
18. C. Duran, S. Trolier-Mckinstry, G.L. Mesing, J. Am. Ceram. Soc. **83**, 2203 (2000)
19. I.E. Gonenli, G.L. Messing, J. Eur. Ceram. Soc. **21**, 2495 (2001)
20. Y. Kan, P. Wang, Y. Li, Y.-B. Cheng, D. Yan, J. Eur. Ceram. Soc. **23**, 2163 (2003)
21. J.L. Jones, S.C. Vogel, E.B. Slamovich, K.J. Boman, Scr. Mater. **51**, 1123 (2004)
22. J.A. Horn, S.C. Zhang, G.L. Messing, S.T. Mckinstry, J. Am. Ceram. Soc. **82**, 921 (1999)
23. H. Amorin, A.L. Kholkin, M.E.V. Costa, J. Eur. Ceram. Soc. **25**, 2453 (2005)
24. M. Kimura, H. Ogawa, D. Kuroda, T. Sawada, Y. Higuchi, H. Takagi, Y. Sakabe, IEEE International Symposium on Applications of Ferroelectrics **4393356**, 645 (2007)
25. S. Kawada, H. Ogawa, M. Kimura, K. Shiratsuyu, H. Niimi, Japanese J.Appl. Physics, Part 1 **44**(9B), 7050 (2005)
26. S. Kawada, H.Ogawa, M.Kimura, K.Shiratsuyu, H.Niimi. Japanese J. Appl. Physics,Part 1: 45 (9 B), 7455(2006)
27. Y. Shimakawa, Y. Kubo, Y. Nakagawa, S. Goto, T. Kamiyama, H. Asano, F. Izumi, Phys. Rev. B **61**, 6559 (2000)
28. J. Barbier, L.M.D. Cranswick, J. Solid State Chem. **179**, 3958 (2006)
29. K. Majhi, K.B.R. Varma, J. Non-Crystal. Solids **354**, 4543 (2008)
30. B. Harihara Venkataraman, K.B.R. Varma, J. Phys. Chem. Solids **64**, 2105 (2003)
31. S. Huang, C. Feng, L. Chen, Q. Wang, J. Am. Ceram. Soc. **89**, 328 (2005)
32. X.G. Tang, X.X. Wang, K.-H. Chew, H.L.W. Chan, Solid State Commu. **136**(2), 89 (2005)
33. R.L. Withers, J.G. Thompson, A.D. Rae, J. Solid State Chem. **94**, 404 (1991)
34. M. Venet, I.A. Santos, J.A. Eiras, D. Garcia, Solid State Ion. **177**, 589 (2006)
35. Z. Ujma, M. Adamczyk, J. Handerek, J. Eur. Ceram. Soc. **18**, 2201 (1998)